Uncertainties in MODIS-Derived *Ulva Prolifera* Amounts in the Yellow Sea: A Systematic Evaluation Using Sentinel-2/MSI Observations

Lin Qi, Menghua Wang, and Chuanmin Hu

***Abstract*— Uncertainties are an integral part of remote sensing data products in order to quantify changes, yet due to patchiness and spatial heterogeneity, it is difficult to use field measurements to estimate uncertainties in the satellite-derived *Ulva prolifera* (*U. prolifera*, also called green tides) amounts in the Yellow Sea. This is perhaps why such estimates are missing in nearly all remote sensing literature on *U. prolifera* mapping. Here, by comparing all available data collected by the Moderate Resolution Imaging Spectroradiometer (MODIS) on the Terra/Aqua satellites and the MultiSpectral Instrument (MSI) on the Sentinel-2A/2B satellites for the period of 2015–2022, we evaluate uncertainties in the MODIS-derived *U. prolifera* amounts. The relative uncertainties are found to decrease with increasing *Ulva* amounts in individual images, ranging from 58.8% for *Ulva* areal coverage (after pixel unmixing) of <50 km^2 to 8.7% for *Ulva* areal coverage of >200 km^2. Such uncertainties decrease in the monthly composite data products because of the increased number of observations, reducing to 3% in the total *Ulva* amount during the peak months. Such uncertainty estimates, in relative terms, are expected to serve as a reference when interpreting temporal changes in long-term *Ulva* estimates derived from satellite data.**

***Index Terms*— Biomass, coverage, green tides, Moderate Resolution Imaging Spectroradiometer (MODIS), MultiSpectral Instrument (MSI), remote sensing, *Ulva prolifera* (*U. prolifera*), Visible Infrared Imaging Radiometer Suite (VIIRS), Yellow Sea.**

I. Introduction

STARTING in the late 2000s, blooms of the green macroalgae *Ulva prolifera* (*U. prolifera*, often called green tides) began to occur every spring–summer in the western Yellow Sea (YS, Fig. 1) (see [1], [2]), and in certain years, they represented the largest green macroalgae blooms around the world (see [3], [4]). The blooms were mostly regarded as a coastal nuisance because of their adverse impacts on the coastal environments and local economy. For this reason, governmental agencies have spent significant efforts and resources on green tide mitigation, including control of *U. prolifera* sources, nutrient reductions, and physical removal of *U. prolifera* at sea (e.g., [5], [6]). Meanwhile, numerous studies have been published on their spatial/temporal patterns, origins, and potential causes (e.g., [4], [7], [8], [9]).

Of the various methods to study the *U. prolifera* green tides, satellite remote sensing is the most effective one to reveal their spatial patterns and temporal changes from which potential causes and consequences may be inferred. This is because of the synoptic and frequent coverage from satellite measurements, as well as the contributions of surface floating *U. prolifera* to the satellite-detected signals. Between 2008 and the present, more than 50 peer-reviewed papers have used satellite remote sensing to estimate *U. prolifera* amounts (see bibliography reviewed by Hu et al. [10]), some of which also showed multiyear changes (e.g., [2], [4], [11], [12], [13]).

However, a critical component is missing in nearly all these studies: uncertainty estimates. Although such estimates are an integral part of any remote sensing data product, they are missing mainly because of the difficulties in using field measurements to evaluate satellite-derived *U. prolifera* amounts. Such difficulties are due to the strong patchiness and heterogeneity in *U. prolifera* distributions where most satellite image pixels are only partially covered by *U. prolifera*, which also drift with winds and currents. Unlike evaluations of the traditional ocean color data products, it is essentially impossible to find a "matching pair" to compare an image pixel with the corresponding field measurement, and it is also difficult to collect all *U. prolifera* within a large region and then compare with colocated image pixels within the same region.

One alternative way to estimate uncertainties is through cross-sensor comparison and specifically to use high spatial resolution satellite data to evaluate uncertainties from coarse-resolution satellite data. This is because the two measurements have different sensor characteristics (spectral bands, signal-to-noise ratios (SNRs), and solar-sensor viewing geometry) that can be regarded as being independent. Indeed, Hu et al. [11], Lu et al. [14], and Wang et al. [15] used such a cross-sensor comparison method to estimate relative uncertainties in the *U. prolifera* amounts derived from individual coarse-resolution images. However, these results were based on a limited number of images, making it difficult to have statistically meaningful conclusions.

Manuscript received 9 February 2023; revised 12 April 2023; accepted 27 April 2023. Date of publication 8 May 2023; date of current version 30 May 2023. This work was supported in part by the Joint Polar Satellite System Program and under Grant ST13301CQ0050/1332KP22FNEED004 and in part by the U.S. NASA under Grant 80NSSC20M0264 and Grant 80NSSC21K0422. *(Corresponding author: Lin Qi.)*

Lin Qi is with the NOAA Center for Satellite Applications and Research, College Park, MD 20740 USA, and also with Global Science and Technology Inc., Greenbelt, MD 20770 USA (e-mail: lin.qi@noaa.gov).

Menghua Wang is with the NOAA Center for Satellite Applications and Research, College Park, MD 20740 USA (e-mail: menghua.wang@noaa.gov).

Chuanmin Hu is with the College of Marine Science, University of South Florida, Saint Petersburg, FL 33701 USA (e-mail: huc@usf.edu).

Digital Object Identifier 10.1109/LGRS.2023.3272889

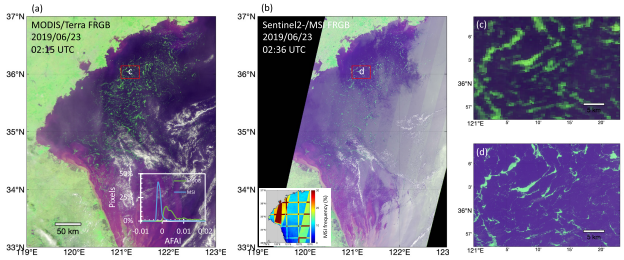

Fig. 1. Comparison of coverage and *U. prolifera* observations over the study region of the western Yellow Sea (33–37°N, 119–123°E) between (a) medium-resolution FRGB image of MODIS/Terra (250 m) and (b) high-resolution FRGB image of MSI (10 m). The images were collected on the same day within 21 minutes. *Ulva* rafts appear as greenish image slicks, and black indicates no data coverage. Two small regions (outlined in red rectangles) are shown in (c) and (d), respectively, whose histogram distributions of AFAI are shown in the inset panel (a). The MSI coverage frequency within a month is shown in the inset panel (b), where the vertical- and horizontal-colored lines indicate overlapping areas of adjacent MSI tiles.

The objective of this letter is to systematically evaluate relative uncertainties in the *U. prolifera* amounts derived from the Moderate Resolution Imaging Spectroradiometer (MODIS) images. MODIS is used here due to its long-term coverage because most published long-term change studies are based on MODIS measurements (see [10]). In the end, we hope to address the question that if a certain year shows more *U. prolifera* than another year, whether the difference is within the uncertainties (therefore, the two years may be regarded as similar) or well beyond the uncertainties.

II. Data and Method

A. MODIS Data and Processing

MODIS data were obtained from the NASA OB. DAAC (https://oceancolor.gsfc.nasa.gov) to: 1) generate false-color red–green–blue (FRGB) images (R: 645 nm; G: 859 nm; B: 469 nm) for visual inspection of image features that are deemed to be *U. prolifera*; 2) extract *U. prolifera* pixels and estimate subpixel *U. prolifera* factional cover (i.e., areal density in %) from alternative floating algae index (AFAI) [16], [17]; 3) find colocated and concurrent MODIS and MultiSpectral Instrument (MSI) image pairs for cross-sensor evaluation and for estimating uncertainties; and 4) generate monthly composites to estimate the monthly mean *U. prolifera* amount, from which long-term time series was generated.

All of the above steps were based on the Rayleigh-corrected reflectance ($R_{\mathrm{rc}}(\lambda)$, dimensionless) generated using MODIS Level-1B data and the SeaDAS software (version 8.0). The use of the FRGB images was to facilitate visual inspection of various image features. In such images, *U. prolifera* features appear greenish because of the enhanced reflectance at the near-infrared (NIR) 859-nm band. An example is shown in Fig. 1(a).

Cloud masking was based on the magnitude and spectral shape of $R_{\mathrm{rc}}(\lambda)$ in each pixel (see [13])

$$Cloud\text{-}Masking = where(R_{rc}(488) > a \cap R_{rc}(547) > a \cap R_{rc}(667) > a). \quad (1)$$

Here, for MODIS $R_{\mathrm{rc}}(\lambda)$, $a = 0.06$. Then, delineation *U. prolifera* features and estimating subpixel fractional cover were based on the $R_{\mathrm{rc}}(\lambda)$-derived AFAI (see [2])

$$\mathrm{AFAI} = R_{\lambda_2} - \left[R_{\lambda_1} + \frac{\lambda_2 - \lambda_1}{\lambda_3 - \lambda_2} \times \left(R_{\lambda_3} - R_{\lambda_1}\right)\right] \quad (2)$$

where $\lambda_1 = 667$ nm, $\lambda_2 = 748$ nm, and $\lambda_3 = 869$ nm. The subpixel fractional cover (χ from 0% to 100%) was estimated through linear unmixing using lower bound threshold (AFAI_l, corresponding to 0% *U. prolifera* within a pixel) and upper bound threshold (AFAI_h, corresponding to 100% *U. prolifera* within a pixel) (see [10])

$$\chi_i = \frac{\mathrm{AFAI}_i - \mathrm{AFAI}_l}{\mathrm{AFAI}_h - \mathrm{AFAI}_l} \times 100\%. \quad (3)$$

Here, the subscript i refers to the ith valid pixel. The original images were converted into 4-km grids, where mean *U. prolifera* areal density in each 4-km grid was calculated as

$$f = \frac{1}{N_t}\sum_{i=1}^{N_t}\chi_i \quad (4)$$

where N_t is the number of valid pixels in the grid. Similar to χ_i, f also ranges between 0% and 100%. In practice, because most of the valid pixels have low χ_i values due to the large pixel size, f is often lower than a few percent. The above processes are shown in Fig. 2 (top row), where additional cloud masking from the colocated and concurrent MSI image was also used to show the commonly valid pixels. Integration of f over all grids, after accounting for the grid size, led to the estimate of the total *U. prolifera* coverage (km^2) from the image. Then, the coverage was converted to biomass using a calibration constant of 1.94 kg m^{-2} (see [18]). Note that such coverage or biomass estimates from individual images are independent of the grid size (either 1- or 4-km), but the use of the 4-km grid can facilitate visualization of image features in limited space.

Equation (4) was also used to generate monthly composite images, where in each 4-km grid of the composite image, N_t is the number of valid pixels in the grid within the month. In this way, f is regarded as the mean *U. prolifera* areal density during the month, and integration of f over all grids led to the estimate of the mean *U. prolifera* coverage (km^2) during the month, which was then converted to the mean *U. prolifera* biomass. This process follows the protocol used by NASA to generate monthly data products at 4-km resolution using 1-km data.

B. MSI Data and Processing

MSI top-of-atmosphere (TOA) reflectance data at multiple spectral bands were downloaded from the European Space Agency (ESA) through Google Earth engine (https://developers.google.com/earth-engine/datasets/catalog/COPERNICUS_S2_HARMONIZED). The spectral bands used in this study include 490 nm (B2), 555 nm (B3), 665 nm (B4), 740 nm (B6), and 865 nm (B8A). Both Sentinel-2A (2015–present) and Sentinel-2B (2017–present) were used, which provided a combined five-day revisit frequency at a local time of ~10:30 A.M. The MSI images have a nominal resolution of 10 and 20 m for most bands. Between

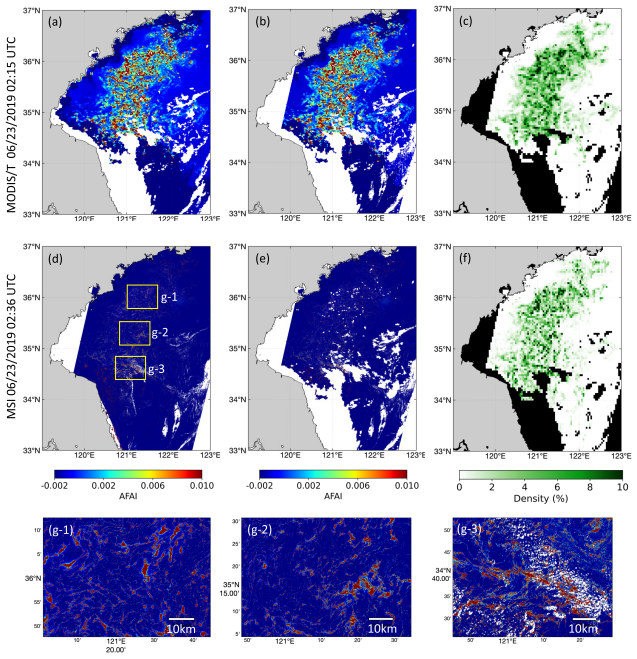

Fig. 2. Illustration of how to obtain a matching pair between MODIS (top row) and MSI (middle row) from the two images shown in Fig. 1. From left to right: (a) AFAI images after masking clouds and other invalid data (white) from sensor-specific data, (b) AFAI images after masking clouds and other invalid data (white) from both images (i.e., combination of the two masks), and (c) *Ulva* density in each 4-km grid where the invalid data are masked as black. Land is shown in gray in (a)–(f). The two images in (c) and (f) over their common valid pixels (white and greenish colors) are considered an image pair. The lack of features in the MSI images [(d) and (e)] is due to the visual illusion effect in presenting high-resolution images in a limited space. At full resolution, these image features appear much clearer as shown in (g-1)–(g-3). Use of the 4-km grid does not affect the estimation of total algae coverage from individual images (see Section II-A) but can improve visualization.

2015 and 2021, a total of 4907 MSI tiles covering the study region during the months of June and July, including the peak season of *U. prolifera* outbreaks (see [2], [13]), were mosaiced into 218 images.

The processing steps of MSI images were similar to those of MODIS, except that the last step of generating monthly composite images was omitted due to the low revisit frequency. The MSI FRGB images were generated using the bands of red: 665 nm (B4), green: 865 nm (B8A), and blue: 555 nm (B3). In fact, the MSI AFAI images were produced using the same method (1) with $\lambda_1 = 665$ nm (B4), $\lambda_2 = 740$ nm (B6), and $\lambda_3 = 865$ nm (B8A). Cloud masking was carried out through analysis of spectral shape and magnitude at 490 nm (B2), 555 nm (B3), and 665 nm (B4) bands, same as (1) but with $a = 0.2$. Delineation of *U. prolifera* image features was through a deep learning approach with an overall accuracy of >85%, which was detailed in [19]. The processing steps are shown in Fig. 2 (bottom row), where additional mask from the paired MODIS image was also used to show the commonly valid pixels.

C. Statistics of Paired MODIS and MSI Images

Although MODIS has daily coverage of the study region, MSI only provides images every five days. After removing images with significant cloud cover, the number of image pairs has been reduced to 113 for the period of 2015–2022 (see Fig. 3). In each image pair, the *U. prolifera* coverage from their commonly valid pixels was estimated from each image and compared. The comparison was performed over all image pairs with statistics generated.

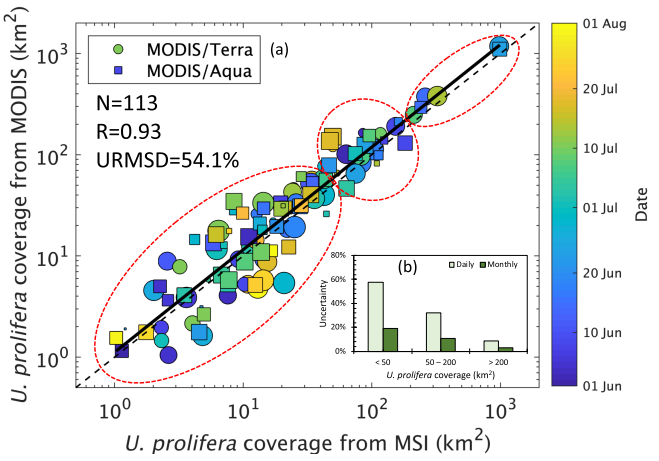

Fig. 3. (a) Comparison between MODIS- and MSI-derived *Ulva* coverage from 113 image pairs collected between 2016 and 2022. The image acquisition date is color coded, while the symbol size indicates the average sensor-zenith angle (3°–70°) from all valid MODIS pixels used in the *Ulva* estimates. The dashed line is the 1:1 line, while the solid line is the best fit between the two datasets. The three dashed ellipses outline the data groups of <50 km^2, 50–200 km^2, and >200 km^2, where relative uncertainties in MODIS estimates decrease with increasing coverage as shown in (b).

III. Results

For the study region shown in Fig. 1(a), MSI cannot cover the entire region due to its relatively narrow swath of 290 km [see Fig. 1(b)] compared with MODIS's 2330 km. This narrower swath led to less frequent coverage (see Fig. 1(b) inset), which is also the reason why it is impractical to generate monthly composite MSI images. Nevertheless, the much finer resolution (10–20 m) led to much sharper image features [see Fig. 1(d)] than those enabled by MODIS [see Fig. 1(c)], which is the reason why MSI serves as an excellent independent data source to evaluate uncertainties in the MODIS-derived *U. prolifera* amounts. This is despite the fact that their AFAI distributions are different (see Fig. 1(a) inset) due to their differences in spectral bands and bandwidths. Such differences were taken care of by their sensor-specific delineating and unmixing algorithms, as shown in Fig. 2.

As an example, Fig. 2 shows the comparison of AFAI and *U. prolifera* density maps derived from the paired MODIS and MSI images, with their original FRGB images presented in Fig. 1. In this example, *U. prolifera* image features are revealed clearly in both MODIS and MSI AFAI images. The reason why the latter appear less clear is due to the MSI high resolution that makes the features appear much smaller in the icon images of Fig. 2(d) and (e). When the images are displayed at full resolution [a subregion is shown in Fig. 2(g)], these image features become much clearer, similar to the contrasting effect shown in Fig. 1(c) and (d). Indeed, after aggregating all pixels into the 4-km grids, the distribution patterns of *U. prolifera* density appear very similar between MODIS and MSI [see Fig. 2(c) and (f)].

Similar observations were made for each image pair, with a total of 113 pairs obtained between 2015 and 2022 [see Fig. 3(a)]. Overall, although there appears a slight systematic positive bias in MODIS data (i.e., the fitting line is slightly above the 1:1 line), strong agreement was found between MODIS- and MSI-derived *U. prolifera* amounts, with $R = 0.93$ and unbiased root-mean-square difference (uRMSD) of 54.1%. Here, uRMSD is defined as

$$\text{uRMSD} = \sqrt{\frac{1}{N}\sum\left(\frac{Y_i - X_i}{0.5 \times (Y_i + X_i)}\right)^2} \tag{5}$$

where Y_i and X_i represent MODIS- and MSI-derived *U. prolifera* amount from an image pair, respectively. The uRMSD value decreases with increasing *U. prolifera* amount, from 58.7% for <50 km^2, 46.3% for 50–200 km^2, to 22.3% for >200 km^2.

The summary results in Fig. 3(a) form the basis to estimate uncertainties in the MODIS-derived *U. prolifera* amounts. Ideally, uncertainties should be evaluated against the ground "truth" [20]. In practice, however, the truth is often unknown because even field measurements are not error-free. Here, the reference is from MSI measurements that are also subject to large uncertainties. The fitting line in Fig. 3(a) is regarded as the "truth," where uncertainties were estimated as the uRMSD difference between MODIS data and the fitting line. Such estimated uncertainties are 52.2% for the entire data range, and 58.8%, 37.6%, and 8.7% for the three subranges [see Fig. 3(b)].

The uncertainties estimated above are for *U. prolifera* amounts estimated from individual images. In the monthly composite images, because of the multiple measurements at each location, the uncertainties are expected to decrease following the $1/(N)^{1/2}$ rule. This is because the relative difference between MODIS and the fitting line appears to be normally distributed. The number of valid 1-km pixels used in calculating the monthly composites generally falls in the range of 80–200 for each 4-km grid, equivalent to about nine cloud-free observations in a typical 1-km location. Therefore, at the monthly scale, uncertainties are expected to be reduced by a factor of 3 from daily images (Fig. 3(b), dark green bars). For the peak months with *U. prolifera* amount > 200 km^2, this suggests a relative uncertainty of 8.7%/3 $\approx$ 3%.

IV. Discussion

The difficulty in validating the remotely estimated amounts of floating matters is not restricted to *U. prolifera* but also applied to oil slicks and all other types of floating matters such as *Sargassum sp.* and marine debris. The use of cross-sensor comparison as a consistency measure to estimate relative uncertainties is not new (e.g., [11], [14], [15]), but it is difficult to draw statistically meaningful conclusions with just a number of limited images. In this regard, the systematic evaluation here using all available MODIS and MSI image pairs, which are collected under different measurement conditions (e.g., solar- and/or sensor-zenith angles) in different *U. prolifera* growing phases, led to uncertainty estimates that may serve as a reference to better interpret temporal changes. For example,

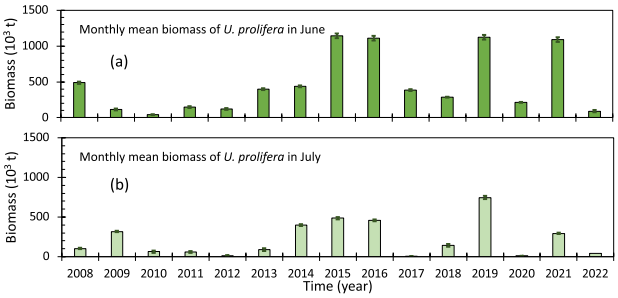

Fig. 4. Monthly mean biomass (in metric tons) of *U. prolifera* derived from MODIS monthly composite images between 2008 and 2022 for the month of (a) June and (b) July. Vertical bars represent uncertainties after multiplying the relative uncertainties in (b) by the monthly amount.

in the 2008–2022 monthly time series of *U. prolifera* amount (see Fig. 4), although annual fluctuation patterns are clear, it is difficult to know whether the difference between certain years is statistically significant. With the knowledge of uncertainties (black vertical bars in Fig. 4), the interpretation becomes straightforward. For example, there is no statistical difference between 2015 and 2016 in either June or July. In contrast, while the result in 2019 shows no statistical difference from that in 2021 in June because their difference is within two times the uncertainties, a statistical difference is found in July because their difference between 2019 and 2021 is $\gg$ two times the uncertainties.

The summary results in Fig. 3(a) may appear puzzling, as one would expect higher estimates from MSI than those from MODIS. This expectation is due to the much-improved spatial resolution (10–20 m) that would enable the detection of the otherwise undetectable small *U. prolifera* mats, leading to more *U. prolifera* detection from MSI images. However, what was observed is against this intuition, as all data points are rather equally spaced around the 1:1 line with MODIS even showing a slight positive bias. Such a puzzling result is due to several reasons. First, as shown in [11] and [14], the NIR reflectance of a *U. prolifera* mat can exceed the selected upper-bound threshold. For MODIS, such an "overflow" is interpreted as coming from nearby water within the same pixel, causing higher estimates from the pixel. Second, MSI images are very noisy due to the sensor's relatively low SNRs over water (e.g., ~33 at the 740-nm band [19], [21]). The noisy data led to many weak features that are undetectable in the MSI images. However, such weak features can be detected more easily if the 10-m resolution pixels are aggregated to form coarser-resolution images with much higher SNRs (see [22, Fig. 10]). Both effects can lead to higher estimates from MODIS images than those from MSI images, but they appear to be compensated by additional *U. prolifera* mats detected only from MSI images, thus leading to the scattered results in Fig. 3(a). Such scattered results can also explain why the use of just a few images in cross-sensor evaluations can lead to results that are not statistically meaningful.

Needless to say, the uncertainties estimated here are in relative terms, representing a measure of self-consistency. However, because studies of temporal changes are also on a relative scale, a measure of self-consistency is sufficient to

quantify the changes as well as to investigate the causes and consequences of such changes. In this regard, the estimated uncertainties in Fig. 4 are expected to serve as a reference when interpreting temporal changes in future time series analysis.

Finally, the uncertainty estimates are for MODIS measurements because of their long-term data availability. Other coarse-resolution multiband sensors, such as the Visible Infrared Imaging Radiometer Suite (VIIRS, from 2011 to present), have shown consistent performance in detecting and quantifying floating macroalgae (see [23]) and therefore are expected to have similar uncertainties as presented here.

V. Conclusion

Despite the extensive use of satellite remote sensing in mapping *U. prolifera* green tides in the Yellow Sea, uncertainties in the satellite-derived *U. prolifera* amounts are generally unknown due to technical difficulties in relating field and satellite measurements. Through a systematic evaluation of 113 paired MODIS and MSI images (from 4907 MSI tiles) for the period of 2015–2022, we quantified their relative differences, which decreases with increasing *U. prolifera* amounts. These differences form the basis to quantify uncertainties in the MODIS-derived *U. prolifera* amounts from both daily and monthly composite images, which are then used to interpret the long-term *U. prolifera* changes. While this study is restricted to *U. prolifera* in the Yellow Sea, the approach is expected to be extendable to other floating matters in other regions such as *Sargassum horneri* in the East China Sea and *Sargassum fluitans/natans* in the Caribbean Sea.

Acknowledgment

The authors thank two anonymous reviewers for their valuable comments. The scientific results and conclusions, as well as any views or opinions expressed herein, are those of the author(s) and do not necessarily reflect those of NOAA or the Department of Commerce.

References

[1] D. Liu, J. K. Keesing, Q. Xing, and P. Shi, "World's largest macroalgal bloom caused by expansion of seaweed aquaculture in China," *Mar. Pollut. Bull.*, vol. 58, no. 6, pp. 888–895, Jun. 2009.

[2] L. Qi et al., "Climate and anthropogenic controls of seaweed expansions in the east China Sea and Yellow Sea," *Geophys. Res. Lett.*, vol. 49, no. 19, Oct. 2022, doi: 10.1029/2022GL098185.

[3] X. Liu, Z. Wang, and X. Zhang, "A review of the green tides in the Yellow Sea, China," *Mar. Environ. Res.*, vol. 119, pp. 189–196, Aug. 2016.

[4] Q. Xing et al., "Monitoring seaweed aquaculture in the Yellow Sea with multiple sensors for managing the disaster of macroalgal blooms," *Remote Sens. Environ.*, vol. 231, Sep. 2019, Art. no. 111279.

[5] Z. Xu, W. Meng, S. Li, and J. Shan, "Residents' preference for the management of green tides and its determinants: The evidence from Qingdao, China," *Ocean Coastal Manage.*, vol. 233, Feb. 2023, Art. no. 106445.

[6] Y. Yang, J. Boncoeur, S. Liu, and P. Nyvall-Collen, "Economic assessment and environmental management of green tides in the Chinese Yellow Sea," *Ocean Coastal Manage.*, vol. 161, pp. 20–30, Jul. 2018.

[7] Y. Huo et al., "Green algae blooms caused by *Ulva prolifera* in the southern Yellow Sea: Identification of the original bloom location and evaluation of biological processes occurring during the early northward floating period," *Limnol. Oceanogr.*, vol. 58, no. 6, pp. 2206–2218, Nov. 2013.

[8] Y. B. Son, B.-J. Choi, Y. H. Kim, and Y.-G. Park, "Tracing floating green algae Blooms in the Yellow Sea and the East China Sea using GOCI satellite data and Lagrangian transport simulations," *Remote Sens. Environ.*, vol. 156, pp. 21–33, Jan. 2015, doi: 10.1016/j.rse.2014.09.024.

[9] Y. Zhang et al., "*Ulva prolifera* green-tide outbreaks and their environmental impact in the Yellow Sea, China," *Nat. Sci. Rev.*, vol. 6, no. 4, pp. 825–838, Jul. 2019, doi: 10.1093/nsr/nwz026.

[10] C. Hu et al., "Mapping *Ulva prolifera* green tides from space: A revisit on algorithm design and data products," *Int. J. Appl. Earth Observ. Geoinf.*, vol. 116, Feb. 2023, Art. no. 103173, doi: 10.1016/j.jag.2022.103173.

[11] L. Hu, K. Zeng, C. Hu, and M.-X. He, "On the remote estimation of *Ulva prolifera* areal coverage and biomass," *Remote Sens. Environ.*, vol. 223, pp. 194–207, Mar. 2019, doi: 10.1016/j.rse.2019.01.014.

[12] Y. Xiao et al., "Remote sensing estimation of the biomass of floating *Ulva prolifera* and analysis of the main factors driving the interannual variability of the biomass in the Yellow Sea," *Mar. Pollut. Bull.*, vol. 140, pp. 330–340, Mar. 2019.

[13] L. Qi, C. Hu, Q. Xing, and S. Shang, "Long-term trend of *Ulva prolifera* blooms in the western Yellow Sea," *Harmful Algae*, vol. 58, pp. 35–44, Sep. 2016, doi: 10.1016/j.hal.2016.07.004.

[14] T. Lu, Y. Lu, L. Hu, J. Jiao, M. Zhang, and Y. Liu, "Uncertainty in the optical remote estimation of the biomass of *Ulva prolifera* macroalgae using MODIS imagery in the Yellow Sea," *Opt. Exp.*, vol. 27, no. 13, pp. 18620–18627, 2019, doi: 10.1364/OE.27.018620.

[15] X. Wang, Q. Xing, and D. An, "Effects of spatial resolution on the satellite observation of floating macroalgae blooms," *Water*, vol. 13, no. 13, p. 1761, 2021.

[16] M. Wang and C. Hu, "Mapping and quantifying Sargassum distribution and coverage in the Central West Atlantic using MODIS observations," *Remote Sens. Environ.*, vol. 183, pp. 350–367, 2016, doi: 10.1016/j.rse.2016.04.019.

[17] C. Hu, "A novel ocean color index to detect floating algae in the global oceans," *Remote Sens. Environ.*, vol. 113, no. 10, pp. 2118–2129, 2009.

[18] L. Hu, C. Hu, and H. Ming-Xia, "Remote estimation of biomass of *Ulva prolifera* macroalgae in the Yellow Sea," *Remote Sens. Environ.*, vol. 192, pp. 217–227, Apr. 2017, doi: 10.1016/j.rse.2017.01.037.

[19] L. Qi and C. Hu, "To what extent can *Ulva* and *Sargassum* be detected and separated in satellite imagery?" *Harmful Algae*, vol. 103, Mar. 2021, Art. no. 102001, doi: 10.1016/j.hal.2021.102001.

[20] S. Dutkiewicz, Ed., "Synergy between ocean colour and biogeochemical/ecosystem models," Int. Ocean Colour Coordinationg Group, Dartmouth, NS, Canada, IOCCG Rep. Ser. 19, 2020, doi: 10.25607/OBP-711.

[21] L. Qi, M. Wang, C. Hu, and B. Holt, "On the capacity of Sentinel-1 synthetic aperture radar in detecting floating macroalgae and other floating matters," *Remote Sens. Environ.*, vol. 280, Oct. 2022, Art. no. 113188, doi: 10.1016/j.rse.2022.113188.

[22] M. Wang and C. Hu, "Automatic extraction of *Sargassum* features from Sentinel-2 MSI images," *IEEE Trans. Geosci. Remote Sens.*, vol. 59, no. 3, pp. 2579–2597, Mar. 2021, doi: 10.1109/TGRS.2020.3002929.

[23] M. Wang and C. Hu, "On the continuity of quantifying floating algae of the Central West Atlantic between MODIS and VIIRS," *Int. J. Remote Sens.*, vol. 39, no. 12, pp. 3852–3869, 2018, doi: 10.1080/01431161.2018.1447161.